Paper ID: TE-011

3D Finite Element Analysis for Heat Transfer in a Solar Collector: Effect of Solar Irradiation

Rehena Nasrin*, Salma Parvin and M.A. Alim

Department of Mathematics, Bangladesh University of Engineering and Technology, Dhaka-1000, Bangladesh
**E-mail: rehena@math.buet.ac.bd*

Abstract

Due to renewable and nonpolluting nature of solar energy it is often used in applications such as electricity generation, thermal heating and chemical processing. "Flat-plate" type solar collectors are the most cost effective. Water based copper nanofluid is used as the heat transfer medium. Three-dimensional heat transfer model is developed in which direct sunlight is incident on transparent glass cover of a flat plate solar collector (FPSC). The governing partial differential equations are solved using finite element method with Galerkin's weighted residual technique. In order to evaluate the temperature and velocity profiles within the collector, the energy balance equation and Navier Stokes equation are solved numerically. Average Nusselt number (Nu) at the heated surface, average temperature (T_{av}), average velocity (V_{av}), mean output temperature (T_{out}) and collector efficiency (η) for both nanofluid and base fluid as well as mid-height temperature (T) for nanofluid through the flat plate solar collector are presented as function of the solar irradiation. It is observed that the solar radiation variation increases the rate of heat transfer and thermal efficiency for nanofluid more than that of pure water. Comparison is also shown between the results obtained using 2D and 3D simulations. Code validation is also shown with the literature available.

Keywords: Flat plate solar collector, finite element method, nanofluid, solar irradiation.

1. Introduction

Solar radiation is radiant energy emitted by the sun. Solar flat plate collectors are commonly used for domestic and industrial purposes and have the largest commercial application amongst the various solar collectors. This is mainly due to simple design as well as low maintenance cost. The heat transfer rate per unit area as thermal radiation is called radiative heat flux. The fluids with solid-sized nanoparticles suspended in them are called "nanofluids". Applications of nanoparticles in thermal field are to augment warmth transport from solar collectors to luggage compartment tanks, to pick up proficiency of coolants in transformers.

Numerical simulation was carried on a solar flat plate collector using [1-2]. Manjunath et al. [3] analyzed three dimensional conjugate heat transfers through unglazed solar flat plate collector. They used finned tubes and the heat transfer simulation due to solar irradiation to the fluid medium, increased with an increase in the mass flow rate. Vestlund [4] studied gas-filled flat plate solar collector. The gases examined were argon, krypton and xenon in his thesis paper. CFD analysis of solar flat plate collector was conducted by [5-7] where the numerical results obtained using the experimentally measured temperatures are compared to the temperatures determined by the CFD model. Struckmann [8] and Kalogirou [9] conducted project and survey reports on solar thermal collectors respectively. Very recently, Nasrin and Alim [10-12] developed a semi-empirical relation for forced convective analysis through a solar collector. A new correlation was derived from their obtained results and it was easy to use heat transfer purposes.

From the above literature review it is mentioned that a very few 3D numerical studies have been completed using traditional fluid that is water, gas, air etc. The overall goal of this study is to numerically simulate 3D model of heat transfer by nanofluids through a flat plate solar collector. The investigation is to be carried out at different values of solar irradiation (I) using 2% concentrated water/Cu nanofluid as well as water.

2. Formulation

The glass top surface is exposed to solar irradiation. It is made up of borosilicate which has thermal conductivity of 1.14 W/mK and refractive index of 1.47, specific heat of 750 J/kgK and coefficient of sunlight transmission of 95%. The wavelength of visible light is roughly 0.7 μm. Thickness of glass cover is 0.005m. There is an air gap of 0.005m between glass cover and absorber plate. Length, width and thickness of the absorber plate are 1m, 0.15m and 0.0005m respectively. The riser pipe has inner diameter 0.01 m and thickness 0.0005m. Coefficients of heat absorption and emmision of copper absorber are 95% and 5% respectively. A

trapezium shaped bonding conductance of copper metal is located from middle one-third part of width of the absorber plate. It covers the three-fourth part of the riser pipe. It is as long as the absorber plate and tube. The computation domain is the copper absorber plate containing a fluid passing copper riser pipe with bonding conductance. Figure 1 shows the computational domain in 3D view.

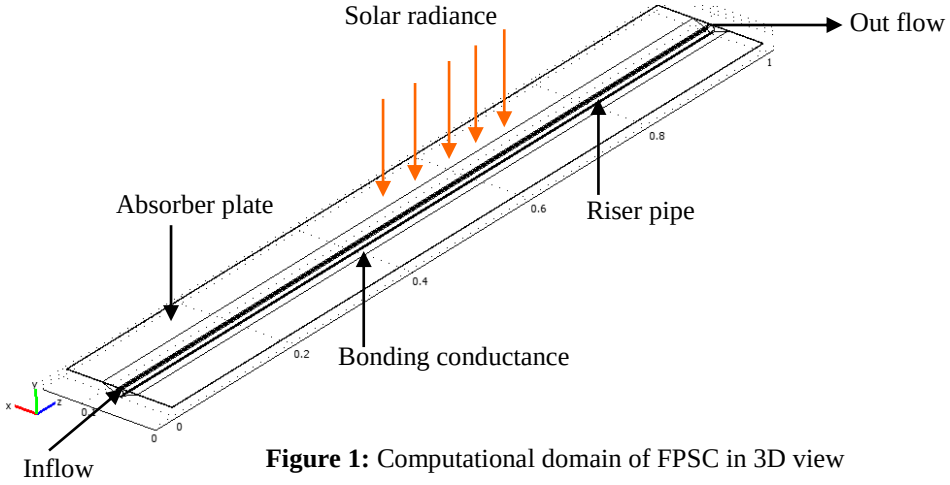

Figure 1: Computational domain of FPSC in 3D view

Let I be the intensity of solar radiation and A be any surface area, then the amount of energy received by any surface is: $Q_i = I.A$ (1)

This equation is modified for solar collector surface as it is the product of the rate of transmission of the cover (τ) and the absorption rate of the absorber (α). Thus, $Q_{recv} = I(\tau\alpha)A$ (2)

Some heat is lost to the atmosphere by convection and radiation process. The rate of heat loss (Q_{loss}) depends on the collector overall heat transfer coefficient (U_l) and the collector temperature.

$$Q_{loss} = U_l A(T_{col} - T_{amb}) \quad (3)$$

The rate of useful energy extracted by the collector (Q_{usfl}) is: $Q_{usfl} = Q_{recv} - Q_{loss} = I(\tau\alpha)A - U_l A(T_{col} - T_{amb})$ (4)

Another form of rate of heat extraction from the collector can be measured as $Q_{usfl} = mC_p(T_{out} - T_{in})$ (5)

where m, C_p, T_{in} and T_{out} are the mass flow rate per unit area, the specific heat at constant pressure, inlet and outlet fluid temperatures respectively.

To calculate the collector average temperature is difficult. The equation (4) may not be convenient. It is convenient to define a quantity that relates the actual useful energy gain of a collector to the useful gain if the whole collector surface is at the fluid inlet temperature. This quantity is known as "the collector heat removal factor (F_R)" and is expressed as: $F_R == \dfrac{mC_p(T_{out} - T_{in})}{A\left[I(\tau\alpha) - U_L(T_{in} - T_{amb})\right]}$ (6)

The maximum possible useful energy gain in a solar collector occurs when the whole collector is at the inlet fluid temperature. The actual useful energy gain (Q_{usfl}), is found by multiplying the collector heat removal factor (F_R) by the maximum possible useful energy gain. Thus equation (4) can be modified as follows:

$$Q_{usfl} = F_R A\left[I(\tau\alpha) - U_L(T_{in} - T_{amb})\right] \quad (7)$$

Equation (7) is known as the "**Hottel-Whillier-Bliss equation"**. The heat flux per unit area of absorber surface (q) is now denoted as $\dfrac{Q_{usfl}}{A} = q = I\tau\alpha - U_L(T_{in} - T_{amb})$. The 3D governing equations are as follows

$$\frac{\partial u}{\partial x} + \frac{\partial v}{\partial y} + \frac{\partial w}{\partial z} = 0 \quad (8)$$

$$\rho_{nf}\left(u\frac{\partial u}{\partial x} + v\frac{\partial u}{\partial y} + w\frac{\partial u}{\partial z}\right) = -\frac{\partial p}{\partial x} + \mu_{nf}\left(\frac{\partial^2 u}{\partial x^2} + \frac{\partial^2 u}{\partial y^2} + \frac{\partial^2 u}{\partial z^2}\right) \quad (9)$$

$$\rho_{nf}\left(u\frac{\partial v}{\partial x} + v\frac{\partial v}{\partial y} + w\frac{\partial v}{\partial z}\right) = -\frac{\partial p}{\partial y} + \mu_{nf}\left(\frac{\partial^2 v}{\partial x^2} + \frac{\partial^2 v}{\partial y^2} + \frac{\partial^2 v}{\partial z^2}\right) \quad (10)$$

$$\rho_{nf}\left(u\frac{\partial w}{\partial x} + v\frac{\partial w}{\partial y} + w\frac{\partial w}{\partial z}\right) = -\frac{\partial p}{\partial z} + \mu_{nf}\left(\frac{\partial^2 w}{\partial x^2} + \frac{\partial^2 w}{\partial y^2} + \frac{\partial^2 w}{\partial z^2}\right) \quad (11)$$

$$u\frac{\partial T}{\partial x}+v\frac{\partial T}{\partial y}+w\frac{\partial T}{\partial z}=\frac{\alpha_{nf}}{\alpha_f}\frac{1}{Pr}\left(\frac{\partial^2 T}{\partial x^2}+\frac{\partial^2 T}{\partial y^2}+\frac{\partial^2 T}{\partial z^2}\right) \tag{12}$$

$$\left(\frac{\partial^2 T_a}{\partial x^2}+\frac{\partial^2 T_a}{\partial y^2}+\frac{\partial^2 T_a}{\partial z^2}\right)=0 \tag{13}$$

Here, $\alpha_{nf}=k_{nf}\left/\left(\rho C_p\right)_{nf}\right.$ is the thermal diffusivity, $\rho_{nf}=(1-\phi)\rho_f+\phi\rho_s$ is the density, $\left(\rho C_p\right)_{nf}=(1-\phi)\left(\rho C_p\right)_f+\phi\left(\rho C_p\right)_s$ is the heat capacitance, $\mu_{nf}=\dfrac{\mu_f}{(1-\phi)^{2.5}}$ is the viscosity of Brinkman model [13], $k_{nf}=k_f\dfrac{k_s+2k_f-2\phi\left(k_f-k_s\right)}{k_s+2k_f+\phi\left(k_f-k_s\right)}$ is the thermal conductivity of Maxwell Garnett (MG) model [14] and $Pr=\dfrac{v_f}{\alpha_f}$ is the Prandtl number. The boundary conditions of the computation domain are:

at all solid boundaries of the riser pipe: $u = v = w = 0$, at the solid-fluid interface: $k_f\left(\dfrac{\partial T}{\partial N}\right)_{fluid}=k_a\left(\dfrac{\partial T}{\partial N}\right)_{solid}$, at the inlet boundary of the riser pipe: $T = T_{in}$, $w = w_{in}$, at the outlet boundary: convective boundary condition $p = 0$, at the top surface of the absorber: heat flux $-k_a\dfrac{\partial T_a}{\partial z}=q=I\tau\alpha-U_L\left(T_{in}-T_{amb}\right)$, at the other surfaces of absorber plate: $\dfrac{\partial T_a}{\partial N}=0$, at the outer boundary of riser pipe: $\dfrac{\partial T_a}{\partial N}=0$, at the outer boundary of bonding conductance: $\dfrac{\partial T_a}{\partial N}=0$, where N is the distances either along x or y or z directions acting normal to the surface respectively.

The average Nusselt number at the inner surface of riser pipe is $Nu=\dfrac{\iint_S \overline{Nu}\,ds}{\iint_s dS}=-\dfrac{1}{\pi DL}\dfrac{k_{nf}}{k_f}\iint_S\sqrt{\dfrac{\partial^2\theta}{\partial X^2}+\dfrac{\partial^2\theta}{\partial Y^2}+\dfrac{\partial^2\theta}{\partial Z^2}}\,ds$ where L is the height of absorber tube. The above equations are non-dimensionalized by using the following dimensionless quantities $X=\dfrac{x}{D}$, $Y=\dfrac{y}{D}$, $Z=\dfrac{z}{D}$, $\theta=\dfrac{(T-T_{in})k_f}{qD}$. The instantaneous thermal efficiency of the collector is:

$$\eta=\frac{\text{useful gain}}{\text{available energy}}=\frac{Q_{\text{usfl}}}{AI}=\frac{F_R A\left[I(\tau\kappa)-U_L\left(T_{in}-T_{amb}\right)\right]}{AI}=F_R(\tau\kappa)-F_R U_L\frac{\left(T_{in}-T_{amb}\right)}{I}$$

3. Numerical Modeling

The Galerkin finite element method [15-16] is used to solve the non-dimensional governing equations along with boundary conditions for the considered problem. Conservation equations are solved for the finite element method to yield the velocity and temperature fields for the water flow in the absorber tube and the temperature field for the absorber plate. The equation of continuity has been used as a constraint due to mass conservation and this restriction may be used to find the pressure distribution. Then the velocity components (u, v, w) and temperatures (T, T_a) of governing equations (8-13) are expanded using a basis set. The Galerkin finite element technique yields the subsequent nonlinear residual equations. Gaussian quadrature technique is used to evaluate the integrals in these equations. The non-linear residual equations are solved using Newton–Raphson method to determine the coefficients of the expansions. The convergence of solutions is assumed when the relative error for each variable between consecutive iterations is recorded below the convergence criterion such that $\left|\psi^{n+1}-\psi^{n}\right|\le 1.0\text{e}^{-6}$, where n is the number of iteration and Ψ is a function of any one of u, v, w, T and T_a.

3.1 Mesh Generation

The computational domains with irregular geometries by a collection of finite elements make the method a valuable practical tool for the solution of boundary value problems arising in various fields of engineering. Figure 2 displays the 3D finite element mesh of the present physical domain.

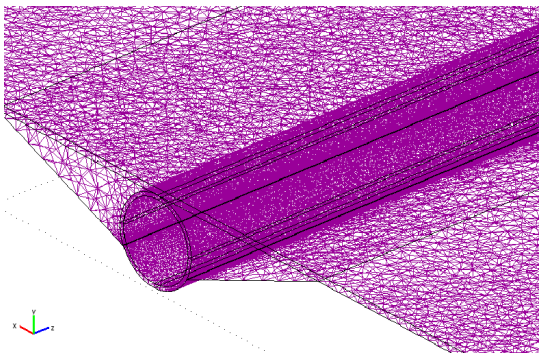

Figure 2: Finite element meshing of FPSC in 3D modeling

3.2 Grid Independent Test

The arrangement of discrete points throughout the domain is simply called a grid. Finite element method can be applied to unstructured grids. This is because the governing equations in this method are written in integral form and numerical integration can be carried out directly on the unstructured grid domain in which no coordinate transformation is required. The mesh is composed of tetrahedral element type with ten nodes in subdomain and triangular element size with six nodes in boundaries. The grid independence test is performed to check validity of the quality of mesh on the solution. There is no significant change in *Nu* taking element size 27,04,288 but it is time consuming. This is shown in Table 1. The computation procedure runs taking 14,20,465 elements in 3D simulation. Thermo-physical properties are shown in Table 2 according to Nasrin *et al.* [17].

Table 1: Grid Sensitivity Test at Pr = 5.8, I = 215 W/m^2, ϕ =2%

Elements	4,51,098	7,26,222	14,20,465	27,04,288
Nu (Nanofluid)	2.12154	2.28451	2.433717	2.433807
Nu (Base fluid)	1.89124	2.00312	2.10124	2.10168
Time (s)	1469.587	3846.507	78381.181	99579.254

Table 2: Thermo physical properties of fluid and nanoparticles

Physical Properties	Fluid phase (Water)	Cu
C_p(J/kgK)	4179	385
ρ (kg/m^3)	997.1	8933
k (W/mK)	0.613	400
α×107 (m^2/s)	1.47	1163.1

3.2 Code Validation

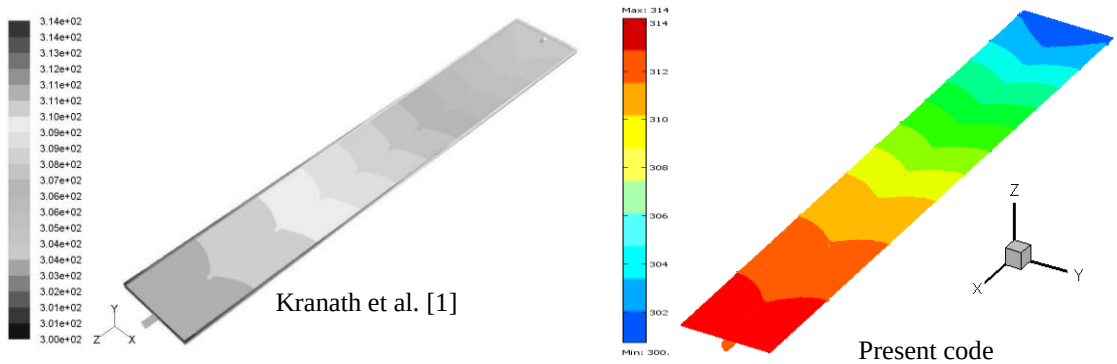

Figure 3: Code validation of temperature contour of absorber plate

The result obtained from present numerical code is verified against the existing result available in the literature. A comparison of temperature contour plot of absorber plate is shown in figure 3 between the result using present code and Kranath et al. [1]. The numerical study is performed at I = 800 w/m^2, inlet velocity = 0.005 m/s, density (copper) = 8900 Kg/m^3, specific heat (copper) = 385 J/kgK, viscosity (water) = 0.000959 Kg/ms,

specific heat (water) = 4179 J/kgK, thermal conductivity (copper) = 387 W/mK and thermal conductivity (water) = 0.6 W/mK. A good agreement is observed from figure 3.

4. Results

The effect of *I* on the temperature interms of slice plot is presented in figure 4 for 2% concentrated water-Cu nanofluid at *Pr* = 5.8and mass flow rate 0.0248Kg/s. The considered values of solar irradiation are *I* (= 200W/m^2, 215W/m^2, 230W/m^2 and 250W/m^2). Different colours of slices indicate different temperatures as shown in the figure. Initially at *I* = 200W/m^2, irradiation is low, temperature of nanofluid at the outlet edge is low. Colour indicates the probable value of nanofluid temperature. The strength of the thermal current activities is much more activated with escalating *I*. Slices illustrate that solar irradiation dominant effect plays a critical role on larger heat flow from absorber walls to the passing fluid through the riser pipe. In the temperature distribution of slice plot for different values of solar irradiation shows that absorber temperature as well as nanofluid outlet temperature increases with rising values of *I*. The values of temperature in slice plots are given in Kelvin unit.

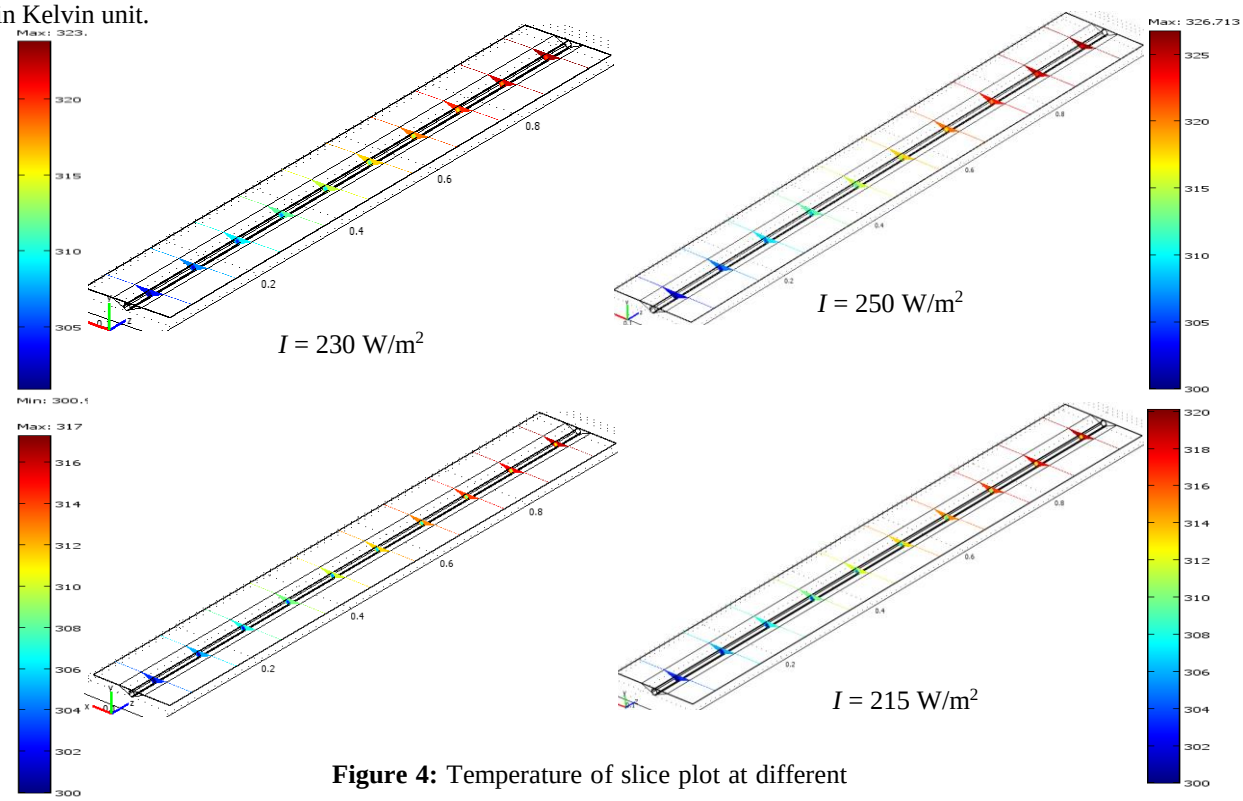

Figure 4: Temperature of slice plot at different

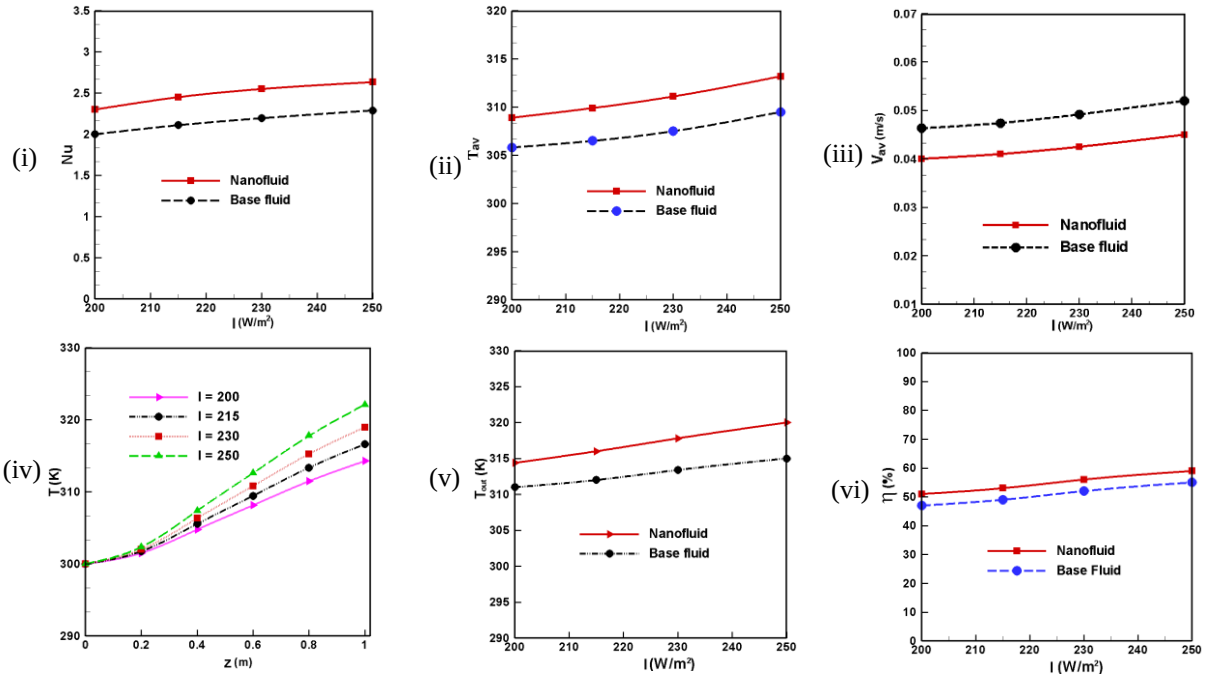

Figure 5: Effect of *I* on (i) mean Nusselt number, (ii) mean temperature, (iii) mean velocity, (iv) mid-height temperature, (v) mean output temperature and (vi) collector efficiency

Figure 5(i)-(vi) expresses the *Nu-I*, T_{av}-*I*, V_{av}-*I*, mid-height temperature of nanofluid, T_{out}-*I* and η-*I* profiles of fluids through a FPSC. The average Nusselt number increases with mounting solar irradiation (*I*). The rate of radiative heat transfer performance enhances 14% and 10% using water-alumina nanofluid and water respectively for rising solar irradiation from 200W/m^2 to 250W/m^2. It is seen from the figure 5(ii) that T_{av} rises sequentially for growing *I*. It is well known that higher values of solar irradiation (*I*) indicate higher temperature of fluids. Due to escalating values of *I* the absorber as well as the riser pipe becomes more heated. As a result fluids can take more heat from hot walls and become hotter. Here base fluid has lower mean temperature than the water-Cu nanofluid. Magnitude of average subdomain velocity (V_{av}) has noteworthy changes with different values of solar irradiation (*I*). It rises consecutively for growing *I*. Clear water has higher velocity than water-copper nanofluid with 2% solid volume fraction. The temperature water-Cu nanofluid at the middle of the riser pipe is depicted in figure 5(iv). The fluid enters from the left inlet and takes heat form solid surfaces of the riser pipe and finally exits from the right outlet of a FPSC. The temperature increases with growing *I*. From the figure 5(v) it is observed that the inlet temperature of fluid is maintained at 300K and then it increases gradually with the contact of heated solid boundaries of the riser pipe. And finally the mean output temperature of nanofluid becomes 314K, 316K, 318K, 320K and water becomes 311K, 312K, 314K, 316K for I = 200 W/m^2, 215 W/m^2, 230 W/m^2 and 250 W/m^2 respectively. By introducing greater solar irradiation (*I*) the collector efficiency increases. More solar irradiance is able to augment heat transfer system through the riser pipe of a FPSC. In this scheme water/copper nanofluid (ϕ = 2%) performs better than clear water (ϕ = 0%). Thermal efficiency enhances from 51%-59% for nanofluid and 47%-55% for water.

5. Conclusion

The 3D numerical study addresses the heat transfer by water/copper nanofluid as well as base fluid through the riser pipe of a FPSC. Solar irradiation has considerable effect on the flow and temperature field. Stronger solar radiation grows up the heat transfer rate, mean outlet temperatureand the thermal efficiency of the FPSC. The mid height temperature of nanofluid increase steadily while passing through the riser pipe for all values of solar radiation. Average velocity is lower for nanofluid than base fluid.

6. Acknowledgement

The present numerical work is done in the Department of Mathematics, Bangladesh University of Engineering & Technology, Dhaka-1000, Bangladesh.

7. References

[1] K.V. Karanth, M.S. Manjunath, N.Y. Sharma, Numerical simulation of a solar flat plate collector using discrete transfer radiation model (DTRM) – a CFD approach, *Proc. of the World Cong. on Engg.*, London, U.K., III, 2011.

[2] OA. Bég, A. Bakier, R. Prasad, SK. Ghosh, Numerical modelling of non-similar mixed convection heat and species transfer along an inclined solar energy collector surface with cross diffusion effects, *World J. of Mech.*, Vol. 1, pp. 185-196, 2011.

[3] M.S. Manjunath, K.V. Karanth, N.Y. Sharma, A comparative CFD study on solar dimple plate collector with flat plate collector to augment the thermal performance, *World Academy of Sci., Engg. and Tech.*, Vol. 6, pp. 10-21, 2012.

[4] J. Vestlund, Gas-filled flat plate solar collector, *Ph. D. Thesis*, Building Services Engg., Dept. of Energy and Environ., Chalmers University of Technology, Gothenburg, Sweden, 2012.

[5] P.W. Ingle, A.A. Pawar, B.D. Deshmukh, K.C. Bhosale, CFD analysis of solar flat plate collector, *Int. J. of Emerg. Techn. and Adv. Engg.*, Vol. 3, No. 4, pp. 337-342, 2013.

[6] S. Basavanna and K.S. Shashishekar, CFD analysis of triangular absorber tube of a solar flat plate collector, *Int. J. Mech. Eng. & Rob. Res.*, Vol. 2, No. 1, pp. 19-24, 2013.

[7] I.A. Tagliafico, F. Scarpa, M.D. Rosa, Dynamic thermal models and CFD analysis for flat-plate thermal solar collectors – a review, *Renew. and Sust. Energy Rev.*, Vol. 2, No. 30, pp. 526-537, 2014.

[8] F. Struckmann, Analysis of a flat-plate solar collector, *Project Report 2008 MVK160 Heat and Mass Transport*, 2008, Lund, Sweden.

[9] Soteris A. Kalogirou, Solar thermal collectors and applications, *Progress in Energy and Combustion Science*, Vol. 30, pp. 231–295, 2004.

[10] R. Nasrin and M.A. Alim, Finite element simulation of forced convection in a flat plate solar collector: Influence of nanofluid with double nanoparticles, J. of Appl. Fluid Mech., Vol. 7, No. 3, pp.543-557, 2014.

[11] R. Nasrin and M.A. Alim, Semi-empirical relation for forced convective analysis through a solar collector, *Solar Energy*, Vol. 105, pp. 455-467, 2014.

[12] R. Nasrin and M.A. Alim, Performance of nanofluids on heat transfer in a wavy solar collector, *Int. J. of Engg., Sci. & Tech.*, Vol. 5, No. 3, pp. 58-77, 2013.

[13] HC. Brinkman, The viscosity of concentrated suspensions and solution, *J. Chem. Phys.*, Vol. 20, pp. 571-581, 1952.

[14] J.C. Maxwell-Garnett, Colours in metal glasses and in metallic films, *Philos. Trans. Roy. Soc. A*, Vol. 203, pp. 385–420, 1904.

[15] C. Taylor, P. Hood, A numerical solution of the Navier-Stokes equations using finite element technique, *Computer and Fluids*, Vol. 1, pp. 73–89, 1973.

[16] P. Dechaumphai, Finite element method in engineering, *2nd ed.*, Chulalongkorn University Press, Bangkok, 1999.

[17] R. Nasrin, S. Parvin and M.A. Alim, Heat transfer and collector efficiency through direct absorption solar collector with radiative heat flux effect, *Numerical Heat Transfer, Part A- Application*, Vol. 68, No. 8, pp. 887-905, 2015.